

1 **Targeting RUNX1 protects against diastolic dysfunction in a two-hit mouse model of heart failure**
2 **with preserved ejection fraction**

3 Ali Ali Mohamed Elbassioni*^{1,2}, Anmar A Raheem*¹, Jian Song¹, Alexander S Johnston¹, Cara Trivett¹,
4 Hong Lin¹, Haobo Zhang¹, Ashley Bradley¹, Erin Higgins¹, Cameron R Thomson¹, Leanne Mooney¹, Yen
5 Chin Koay³, Dylan O'Toole¹, Pawel Herzyk⁴, Colin Nixon⁵, Karen Blyth^{5,6}, Mark Hughes⁵, John F
6 O'Sullivan³, Ninian N Lang¹, Colin Berry¹, Thomas Braun⁷, Gabriele G Schiattarella^{8,9,10}, Mauro Giacca¹¹,
7 Martin W McBride¹, Stuart A Nicklin¹, Ewan R Cameron¹², Christopher M Loughrey^{#1,12}, Eilidh A
8 MacDonald^{#1}.

9
10 *AAME and AAR, as well as #EAM and CML contributed equally to this work and as joint first/last authors
11 can change the order of authorship for the purposes of curriculum vitae.

12 1 British Heart Foundation Glasgow Cardiovascular Research Centre, School of Cardiovascular &
13 Metabolic Health, University of Glasgow, UK

14 2 Department of Cardiothoracic Surgery, Suez Canal University, Egypt

15 3 University of Sydney, NSW Australia

16 4 Glasgow Polyomics, University of Glasgow, Garscube Campus, UK

17 5 Cancer Research UK Scotland Institute, Switchback Road, Bearsden, Glasgow, UK

18 6 School of Cancer Sciences, University of Glasgow, Glasgow, G61 1QH

19 7 Department of Cardiac Development and Remodelling, Max Planck Institute for Heart and Lung
20 Research; Bad Nauheim, Germany

21 8 Deutsches Herzzentrum der Charité (DHZC), Charité -Universitätsmedizin Berlin, Berlin, Germany.

22 2DZHK (German Centre for Cardiovascular Research), Partner Site Berlin, Berlin, Germany.

1 9 Translational Approaches in Heart Failure and Cardiometabolic Disease, Max Delbrück Center for
2 Molecular Medicine in the Helmholtz Association (MDC), Berlin, Germany

3 10 Division of Cardiology, Department of Advanced Biomedical Sciences, Federico II University, Naples,
4 Italy

5 11 King's College London British Heart Foundation Centre, School of Cardiovascular & Metabolic
6 Medicine and Sciences, London, UK

7 12 School of Biodiversity One Health & Veterinary Medicine, University of Glasgow, Garscube Campus,
8 UK

9

10 **ABSTRACT**

11 **Aims:** Heart failure with preserved ejection fraction (HFpEF) continues to increase in prevalence and has
12 limited treatment options. HFpEF is a systemic condition with a broad phenotype including diastolic
13 dysfunction, pulmonary oedema, exercise intolerance, and left ventricular (LV) hypertrophy, collectively
14 resulting in enhanced morbidity and mortality. The transcription factor RUNX1 has recently been identified
15 as a mediator of pathological changes in multiple cardiac diseases, however its role in HFpEF remained
16 unknown.

17 **Methods and Results:** Here we show that inhibition of *Runx1* limits adverse cardiac remodelling in a
18 clinically relevant mouse model of HFpEF. Cardiomyocyte-specific tamoxifen-inducible *Runx1*-deficient
19 mice with HFpEF are protected, with preservation of diastolic function, and attenuation of pulmonary
20 oedema, exercise intolerance, and hypertrophy. Furthermore, targeting *Runx1* in HFpEF by using gene
21 transfer or small molecule inhibitor Ro5-3335 improves diastolic function and reduces pulmonary
22 oedema, both in female and male mice.

23 **Conclusion:** Overall, our research enhances our understanding of RUNX1 in cardiac disease and
24 presents a novel translational target for the treatment of HFpEF.

25

1 Keywords: Heart failure with preserved ejection fraction, metabolic heart failure, diastolic dysfunction,
2 hypertrophy, pulmonary oedema, exercise intolerance

3

4 **Translational Perspective**

5 Heart failure (HF) is a leading cause of death world-wide and traditionally divided into different subtypes
6 according to cardiac ejection fraction (EF). In contrast to HF with reduced EF (HFrEF), there are limited
7 treatment options for HF with preserved EF which is of considerable concern given that HFpEF is
8 projected to become the dominant HF subtype in the future¹. RUNX1 has been demonstrated to play an
9 important role in the development of many cardiac and non-cardiac diseases. As a result, the potential for
10 RUNX1 inhibitors as therapeutic agents across various conditions has become increasingly evident. In
11 this study we established the therapeutic potential of targeting RUNX1 in the context of HFpEF. Targeting
12 RUNX1 using different strategies markedly attenuates the development of diastolic dysfunction and
13 pulmonary oedema in HFpEF. Therefore, RUNX1 represents a novel translational therapeutic target with
14 great potential to address one of the biggest challenges in cardiac research.

15

16 **INTRODUCTION**

17 Heart failure (HF), a complex syndrome in which the heart is unable to meet the metabolic demands of
18 the body, leads to considerable morbidity and mortality worldwide. It is classically categorised by the
19 proportion of blood ejected from the left ventricle (LV) with each beat, the ejection fraction (EF). HF with
20 reduced ejection fraction (HFrEF) has been heavily investigated for many years and there are several
21 treatment options available that reduce mortality². More elusive, however, is HF with *preserved* ejection
22 fraction (HFpEF) which is increasing in prevalence and is poorly understood³. Despite multiple advances
23 in the treatment of HFrEF, the classic HFrEF treatments are not effective for use in HFpEF, resulting in
24 limited therapeutic options⁴. HFpEF is a multimorbidity syndrome, often developing alongside
25 hypertension, metabolic stress, and diabetes, and results in diastolic dysfunction, pulmonary oedema,
26 hypertrophy, and exercise intolerance⁴. HFpEF includes a wide range of clinical phenotypes and

1 pathophysiological heterogeneity⁵. Elucidating molecular or cellular factors contributing to the
2 development of HFpEF is essential and an important step toward identifying therapeutic targets.

3 The master-regulator transcription factor, RUNX1, is minimally expressed in the adult heart but
4 can be reactivated in the context of cardiac pathology. Using preclinical animal model systems, it has
5 been shown to be a mediator and therapeutic target against adverse cardiac remodelling following
6 myocardial infarction (MI) - a major cause of HFrEF⁶⁻⁸, and in a transaortic constriction HFrEF model^{9,10}.
7 Targeting *Runx1* in the post-MI heart results in improved systolic function, calcium handling, and
8 preservation of genes involved in oxidative phosphorylation^{6,7,11}. Large scale analysis of RNAseq studies
9 on human myocardium¹²⁻¹⁸ demonstrates that *Runx1* expression is increased in several cardiac
10 pathologies including myocardial infarction, hypertrophic cardiomyopathy, and dilated cardiomyopathy
11 (Supplemental Figure 1, Supplemental Table 1). Given its established role as a maladaptive regulator in
12 diverse forms of cardiac pathologies, we hypothesised a potential role for RUNX1 in the pathophysiology
13 of HFpEF¹⁹. The aim of this study was to use a preclinical model of HFpEF to interrogate the role of
14 RUNX1 in the development of HFpEF and to identify its potential as a therapeutic target for the treatment
15 of HFpEF.

16 **METHODS**

17 Detailed methods and statistical analysis are presented in the supplemental methods. We used a
18 previously established²⁰, two-hit model (2HM) that combines administration of a high-fat diet (HFD) and
19 inhibition of nitric oxide synthase with N^ω-nitro-L-arginine methyl ester (L-NAME) in drinking water to
20 induce a HFpEF phenotype and compared changes to age-matched controls (CTRL) fed a regular chow
21 diet and normal drinking water²⁰. We utilised cardiomyocyte-specific tamoxifen-inducible *Runx1*-deficient
22 (*Runx1*^{Δ/Δ}) mice and floxed genetic-control mice (*Runx1*^{fl/fl} original line from Gowney *et al*²¹) generated as
23 previously described to reduce *Runx1* expression after being given a single intraperitoneal injection of
24 40mg/kg tamoxifen²². RUNX1 was also targeted by either adeno-associated virus (AAV)-mediated
25 delivery of shRNA (supplemental figure 2) or a small molecule inhibitor of RUNX1, Ro5-3335, as detailed
26 in the supplemental methods. Bulk RNA sequencing and subsequent pathway analysis was performed on
27 LV tissue samples from *Runx1*^{fl/fl} and *Runx1*^{Δ/Δ} mice at baseline and after the 2HM protocol. Using prior

1 biological knowledge from the Ingenuity knowledge base, the cardiotoxicity networks and functional
2 analyses were generated using QIAGEN Ingenuity Pathway Analysis (IPA)
3 (<https://www.qiagenbioinformatics.com/products/ingenuity-pathway-analysis/>). The focus on cardiotoxicity
4 processes considers the likely activation and inhibition of biological processes between the two strain
5 comparisons (2HM-*Runx1^{fl/fl}* compared to CTRL-*Runx1^{fl/fl}* and 2HM-*Runx1^{Δ/Δ}* and CTRL-*Runx1^{Δ/Δ}*) using a
6 Z-score. Differences in Z-scores were identified.

7 **RESULTS**

8 **Runx1 expression in HFpEF**

9 To investigate the involvement of RUNX1 in the pathophysiology of HFpEF, we measured *Runx1* gene
10 expression in cardiomyocytes from our 2HM in C57BL-6N mice. *Runx1*-expression was significantly
11 elevated in 2HM mice compared to CTRL (Supplementary Figure 2) suggesting that Runx1 has potential
12 to drive adverse cardiac remodelling in HFpEF as is the case post-MI.

13 **Effect of cardiomyocyte-specific *Runx1*-deficiency on the development of HFpEF**

14 To evaluate the functional contribution of Runx1, we utilised male *Runx1^{Δ/Δ}* mice and floxed control mice
15 (*Runx1^{fl/fl}*) on the 2HM and CTRL protocols compared to age-matched genetic controls (CTRL-*Runx1^{fl/fl}*: n
16 = 19, CTRL-*Runx1^{Δ/Δ}*: n = 17, 2HM-*Runx1^{fl/fl}*: n = 21, 2HM-*Runx1^{Δ/Δ}*: n = 22, Figure 1a). Each of the two-
17 hits were observed in 2HM-*Runx1^{fl/fl}* and 2HM-*Runx1^{Δ/Δ}* male mice with an increase in body weight ($8.0 \pm$
18 0.9g and $7.0 \pm 0.9\text{g}$, respectively both $P < 0.05$; Figure 1b) and systolic blood pressure (SBP, $22 \pm$
19 10mmHg and $20 \pm 6\text{mmHg}$ respectively, both $P < 0.05$; Figure 1c) over the course of the protocol
20 compared to respective CTRL groups. We confirmed that neither 2HM group had developed HFpEF by
21 assessing whole heart contractile function as measured by fractional shortening *via* echocardiography
22 and ejection fraction from pressure-volume catheters (Supplemental Figure 3a).

23 We then evaluated other key features of the HFpEF phenotype. At the end of the protocol, 2HM-
24 *Runx1^{fl/fl}* mice had developed exercise intolerance, demonstrated by a reduction in running distance
25 compared to CTRL-*Runx1^{fl/fl}* mice ($128 \pm 14\text{m}$ vs. $296 \pm 18\text{m}$ respectively, $P < 0.05$; Figure 1d). 2HM-
26 *Runx1^{Δ/Δ}* mice also had a reduction in running distance compared to their genetic control (2HM-*Runx1^{Δ/Δ}* :

1 192 ± 14m, CTRL-*Runx1*^{ΔΔ}: 327 ± 22m, P<0.05; Figure 1d) however, the exercise intolerance was
2 attenuated because 2HM-*Runx1*^{ΔΔ} mice ran greater distances than 2HM-*Runx1*^{fl/fl} mice (128 ± 14m vs.
3 192 ± 14m, P<0.05; Figure 1d). *Runx1* deficiency also protected mice from developing pulmonary
4 oedema as measured by the wet to dry lung weight. The wet to dry lung weight ratio was increased in
5 2HM-*Runx1*^{fl/fl} compared to in CTRL-*Runx1*^{fl/fl} mice (3.90 ± 0.2 vs. 2.84 ± 0.2, P<0.05; Figure 1e).
6 Conversely, there was no difference between 2HM-*Runx1*^{ΔΔ} and CTRL-*Runx1*^{ΔΔ} mice (3.14 ± 0.2 vs.
7 3.00 ± 0.1; Figure 1e), and 2HM-*Runx1*^{ΔΔ} mice had significantly lower wet to dry lung weight ratio than
8 2HM-*Runx1*^{fl/fl} mice (3.14 ± 0.2 vs. 3.90 ± 0.2, P<0.05; Figure 1e). *Runx1* deficiency was also protective
9 against development of hypertrophy as measured by LV weight. 2HM-*Runx1*^{fl/fl} had increased LV weight
10 compared to CTRL-*Runx1*^{fl/fl} mice (0.111 g ± 0.002 vs. 0.100 g ± 0.003, P<0.05; Figure 1f) whereas 2HM-
11 *Runx1*^{ΔΔ} mice did not have an increase in LV weight compared to CTRL-*Runx1*^{ΔΔ} mice (0.101 ± 0.003
12 vs. 0.098 ± 0.002, P>0.05; Figure 1f). An additional indicator, relevant to concentric hypertrophy, is
13 cardiomyocyte cross-sectional area. In contrast to 2HM-*Runx1*^{fl/fl} animals, 2HM-*Runx1*^{ΔΔ} mice showed no
14 significant increase in the cross-sectional area of cardiomyocytes compared to their relative control group
15 (CTRL-*Runx1*^{fl/fl}: 352 ± 9.9 μm², CTRL-*Runx1*^{ΔΔ}: 323 ± 32.4 μm², 2HM-*Runx1*^{fl/fl}: 482 ± 18.0 μm², 2HM-
16 *Runx1*^{ΔΔ}: 289 ± 24.8 μm²; Figure 1g, Supplemental Figure 3b). Further, posterior and anterior wall
17 thickness measured during systole with M-mode echocardiography was increased in the 2HM-*Runx1*^{fl/fl}
18 mice but not in the 2HM-*Runx1*^{ΔΔ} mice, compared to relevant controls (Supplemental Figure 3c). In
19 addition to hypertrophy, there was a striking preservation of diastolic function in cardiomyocyte-specific
20 *Runx1* knockdown mice, quantified by E to A wave ratio from pulsed-wave Doppler echocardiography.
21 Compared to CTRL-*Runx1*^{fl/fl} and CTRL-*Runx1*^{ΔΔ}, 2HM-*Runx1*^{fl/fl} had a higher E/A ratio whereas the E/A
22 ratio in 2HM-*Runx1*^{ΔΔ} mice was not different from either control group (CTRL-*Runx1*^{fl/fl}: 1.63 ± 0.10,
23 CTRL-*Runx1*^{ΔΔ}: 1.58 ± 0.09, 2HM-*Runx1*^{fl/fl}: 3.75 ± 0.29, 2HM-*Runx1*^{ΔΔ}: 1.67 ± 0.09; Figure 1h,
24 Supplemental Figure 3d). An independent measure of LV chamber stiffness was calculated by fitting the
25 slope of the load-independent end-diastolic pressure-volume relationship (EDPVR) measured using
26 intracardiac pressure-volume catheters. 2HM-*Runx1*^{fl/fl} mice had a steeper EDPVR slope than 2HM-
27 *Runx1*^{ΔΔ} mice, indicating better diastolic function in the 2HM-*Runx1*^{ΔΔ} mice (0.075 ± 0.008 vs. 0.018 ±
28 0.003, P<0.05; Figure 1i, 1j, Supplemental Figure 3e). Peripheral organs were also collected to

1 investigate systemic effects of cardiomyocyte-specific *Runx1*-deficiency. Liver, right kidney, and left kidney
2 weights (all normalised to tibial length) were increased in 2HM-*Runx1^{fl/fl}* compared to CTRL-*Runx1^{fl/fl}* mice
3 but were not different between *Runx1^{ΔΔ}* mouse groups (Supplemental Figure 3f).

4 ***Runx1* RNA interference using adeno-associated virus serotype 9 (AAV9) attenuates diastolic** 5 **dysfunction in HFpEF**

6 Given the striking phenotypic differences observed in 2HM-*Runx1^{ΔΔ}* mice compared to 2HM-*Runx1^{fl/fl}*, we
7 next sought to target RUNX1 using additional approaches to determine whether *Runx1* knockdown could
8 prevent the development of HFpEF. To do this we utilised a viral vector-mediated gene delivery approach
9 with AAV9-*Runx1*-shRNA to knockdown *Runx1* in our 2HM of HFpEF, which we previously validated²².
10 We injected 12-week-old C57BL/6N male mice via the tail vein with AAV9-scramble-shRNA (2HM-AAV9-
11 scram, n = 10) or AAV9-*Runx1*-shRNA (2HM-AAV9-*Runx1*, n = 11) after which mice were placed on the
12 2HM protocol for 8 weeks for comparison to age-matched C57BL/6N mice on the 2HM (2HM-C57N, n =
13 18) or control (CTRL-C57N, n = 13) protocols (Figure 2a). Once again, we confirmed the efficacy of our
14 2HM by measuring changes in body weight (Figure 2b), SBP (Figure 2c), and preservation of fractional
15 shortening from echocardiography (Supplemental Figure 4a) over the duration of the protocol. At the end
16 of the protocol, RNAScope analysis confirmed a significant reduction of *Runx1* expression in 2HM-AAV9-
17 *Runx1* hearts (2HM-AAV9-*Runx1*, n = 6) compared to 2HM-AAV9-scramble-shRNA controls (2HM-AAV9-
18 scram, n = 6) (Supplemental Figure 4b). Targeting *Runx1* with AAV9-*Runx1*-shRNA was effective in
19 preventing a number of the key features of the HFpEF phenotype. Exercise intolerance was observed in
20 all three 2HM groups compared to CTRL-C57N, but with no difference in running distance between 2HM
21 groups (CTRL-C57N: 262 ± 12m, 2HM-C57N: 108 ± 3m, 2HM-AAV9-scram: 108 ± 23m, 2HM-AAV9-
22 *Runx1*: 163 ± 22m; Figure 2d). AAV9-*Runx1* did, however, attenuate the development of pulmonary
23 oedema compared to the other two 2HM groups, quantified by wet to dry lung weight ratio (CTRL-C57N:
24 3.18 ± 0.16, 2HM-C57N: 4.58 ± 0.07, 2HM-AAV9-scram: 4.36 ± 0.12, 2HM-AAV9-*Runx1*: 3.68 ± 0.15;
25 Figure 2e). As with exercise testing, LV/TL was increased in 2HM groups compared to CTRL but was not
26 different between 2HM groups (CTRL-C57N: 4.1 ± 0.2 *10⁻³, 2HM-C57N: 5.0 ± 0.2 *10⁻³, 2HM-AAV9-
27 scram: 5.4 ± 0.2 *10⁻³, 2HM-AAV9-*Runx1*: 4.9 ± 0.2 *10⁻³; Figure 2f). However, cardiomyocyte cross-

1 sectional area of 2HM-AAV9-Runx1 was less than the 2HM-AAV9-scram group (2HM-AAV9-scram: $449 \pm$
2 $10 \mu\text{m}^2$ vs. 2HM-AAV9-Runx1: $308 \pm 23 \mu\text{m}^2$; Figure 2g, Supplemental Figure 4c). Most striking was the
3 preservation of diastolic function by targeting *Runx1* with AAV9. E/A ratio was increased in both 2HM-
4 C57N and 2HM-AAV9-scram groups compared to CTRL-C57N but was not increased in 2HM-AAV9-
5 *Runx1* compared to CTRL-C57N (CTRL-C57N: 1.32 ± 0.10 , 2HM-C57N: 2.55 ± 0.26 , 2HM-AAV9-scram:
6 2.78 ± 0.33 , 2HM-AAV9-Runx1: 1.29 ± 0.12 ; Figure 2h, 2i; the latter figure demonstrating change over
7 time, Supplemental Figure 4d). This was also consistent with EDPVR, which was markedly lower in the
8 2HM-AAV9-Runx1 group compared to 2HM-AAV9-scram (0.077 ± 0.009 vs. 0.019 ± 0.003 , $P < 0.05$;
9 Figure 2j, 2k).

10 **Small molecule inhibition of RUNX1 remedies the HFpEF phenotype**

11 To further translate our findings into a clinically relevant approach, we aimed to identify if inhibition of
12 RUNX1 could reverse the HFpEF phenotype after HFpEF was established using small molecule inhibitor
13 of RUNX1²². 10-12 week-old C57BL/6N strain male mice were placed on the 2HM protocol for 10-12
14 weeks. Prior to drug treatment, *in vivo* parameters were utilised to ensure the HFpEF phenotype had
15 developed and any mice that did not have HFpEF symptoms were excluded so that we were only
16 attempting to treat mice with a phenotype to attenuate. Next, while mice remained on 2HM protocol, we
17 injected small molecule inhibitors of RUNX1, either DMSO or Ro5-3335 every second day during the final
18 two weeks of the protocol prior to collecting end-point measurements and organometrics (Figure 3a).
19 Although RUNX1 inhibition by Ro5-3335 injections did not change exercise tolerance (199.1 ± 50.2 vs.
20 192.5 ± 40.21 , $P > 0.05$; Figure 3b), pulmonary oedema was reduced in 2HM-Ro5-3335 mice compared to
21 2HM-DMSO mice (4.26 ± 0.05 vs. 4.06 ± 0.07 , $P < 0.05$; Figure 3c). As with exercise intolerance,
22 hypertrophy was not changed by Ro5-3335 administration ($4.9 \times 10^{-3} \pm 1.1 \times 10^{-4}$ vs. $5.07 \times 10^{-3} \pm 1.476 \times 10^{-4}$,
23 $P > 0.05$, Figure 3d). Diastolic dysfunction was attenuated in 2HM-Ro5-3335 mice compared to 2HM-
24 DMSO. There was no difference in E/A wave ratio post-injection compared to pre-injection in the 2HM-
25 DMSO mice (2.66 ± 0.35 vs. 2.82 ± 0.15 , $P > 0.05$; Figure 3e, Supplemental Figure 5) whereas the post-
26 injection E/A wave ratio was reduced in the 2HM-Ro5-3335 mice compared to pre-injection,
27 demonstrating diastolic dysfunction was attenuated (1.68 ± 0.14 vs. 2.51 ± 0.16 , $P < 0.05$; Figure 3e,

1 Supplemental Figure 5). This was confirmed using PV loop assessment of diastolic function by EDPVR in
2 2HM-DMSO mice compared to the 2HM-Ro5-3335 group (0.048 ± 0.005 vs. 0.029 ± 0.005 , $P < 0.05$;
3 Figure 3f, 3g).

4 **RNAseq predicts patterns of transcriptional changes consistent with a HFpEF phenotype**

5 To gain broader insight into the role of *Runx1* in HFpEF, we performed bulk RNAseq on analysis on LV
6 tissue samples from *Runx1^{fl/fl}* and *Runx1^{Δ/Δ}* mice both at baseline (day 0, D0) and at the end of the 2HM
7 study. There were not any significantly differentially expressed genes (DEG) between *Runx1^{fl/fl}* and
8 *Runx1^{Δ/Δ}* at D0 and despite the large phenotypic differences, there were only 32 DEG between *Runx1^{fl/fl}*
9 and *Runx1^{Δ/Δ}* mice at week 13 (Supplemental Table 2). However, there were many differences when
10 comparing each strain at week 13 compared to their respective baseline controls. Thus, because the
11 transcriptomic snapshot at the end of the study does not depict the highly different phenotypes, we
12 focussed on comparing the changes from D0 to the end time point within each strain. Using a false
13 discovery rate (FDR) cut-off of ≤ 0.05 and log fold change (logFC) ± 1 , there were 1,866 DEG in 2HM-
14 *Runx1^{fl/fl}* mice at week 13 compared to D0 *Runx1^{fl/fl}* mice (Figure 4a and 4c) and 3,691 DEG at week 13 in
15 2HM-*Runx1^{Δ/Δ}* mice compared to the D0 (Figure 4b and 4c). The majority of DEG were shared between
16 strains (1727 DEG: 92.6% of total DEG for *Runx1^{fl/fl}* and 53.2% of total DEG for *Runx1^{Δ/Δ}*; Figure 4c).
17 Interestingly, the unique changes in the *Runx1^{Δ/Δ}* mice across timepoints may account for the large
18 functional differences observed because there were very few unique changes in the *Runx1^{fl/fl}* mice (Figure
19 4c). Using all significantly DEG in *Runx1^{fl/fl}* and *Runx1^{Δ/Δ}* mice at week 13 compared to baseline, we
20 focused on cardiac toxicity functions defined by IPA software. We compared Z-scores (a statistical
21 measure utilised to determine the significance and directionality of gene expression changes within a
22 given pathway over that time course) from *Runx1^{fl/fl}* (week 13 of 2HM vs D0) and *Runx1^{Δ/Δ}* (week 13 of
23 2HM vs D0). We visualised the impact of *Runx1* deficiency by plotting the difference between Z-scores
24 from *Runx1^{fl/fl}* (2HM vs D0) minus *Runx1^{Δ/Δ}* (2HM vs D0) mice (Z-diff; Figure 4d). Whilst some predictive
25 changes in cardiac toxicity functions demonstrated limited difference in Z-diff (yellow; Figure 4d), the
26 largest differences in Z-score were in congestive heart failure genes and cardiac damage genes. The

1 genes included by IPA in these two cardiac toxicity functions were then plotted using a heat map (Figure
2 4e and f).

3 **Inhibition of *Runx1* in female mice: reversal of HFpEF phenotype**

4 To further increase the relevance and translational impact of our findings, we expanded our study in two
5 ways: we used female mice to ensure clinical relevance; and we waited to intervene with *Runx1* inhibition
6 *via* RNA interference until HFpEF was already established in the mice, to test its utility to reverse adverse
7 cardiac remodelling in HFpEF. It has been demonstrated that it is more difficult to induce a HFpEF
8 phenotype *via* the 2HM in female mice compared to males in young mice²³. Thus, in a cohort of C57-N
9 strain females we waited until they were aged 14 weeks (~40% older than previous data) before placing
10 them on the 2HM protocol with a ramping dose of L-NAME (Figure 5a). Once again, we ensured efficacy
11 of the two hits by measuring body weight and SBP in a female CTRL-C57N group (F-CTRL-C57N, n = 4)
12 compared to a female 2HM-C57N group (F-2HM-C57N, n = 16; Figure 5b, 5c). We utilised our
13 intermediary *in vivo* phenotypic measures exercise intolerance (Figure 5d) and diastolic dysfunction
14 (Figure 5e) to confirm that at the 8-week time point the F-2HM-C57N group had established a HFpEF
15 phenotype. Following this, we split the F-2HM-C57N group into two groups for AAV-mediated gene
16 delivery such that they had consistent starting parameters (Figure 5a). One group was injected with
17 AAV9-scramble-shRNA (F-2HM-AAV9-scram, n = 8) and a second injected with AAV9-*Runx1*-shRNA to
18 knockdown *Runx1* (F-2HM-AAV9-*Runx1*, n = 8). Consistent with the male AAV study, there were no
19 differences in running distance between groups 4 weeks following AAV injection (F-2HM-AAV9-scram:
20 188 ± 8m, F-2HM-AAV9-*Runx1*: 182 ± 17m, p = 0.7560; Figure 5f). We found pulmonary oedema was
21 reduced in the F-2HM-AAV9-*Runx1* compared to F-2HM-AAV9-scram (3.97 ± 0.05 vs 4.29 ± 0.07,
22 respectively, p = 0.0024; Figure 5g) which was consistent with the male data (Figure 2e). Although
23 hypertrophy (measured by LV weight normalised to TL) was not different between the 2HM-AAV-scram
24 and 2HM-AAV-*Runx1* males (Figure 2f), it was reduced in F-2HM-AAV9-*Runx1* compared to F-2HM-AAV-
25 scram (3.1 ± 0.1 *10⁻³ vs 3.6 ± 0.2 *10⁻³, respectively, P<0.05; Figure 5h). Finally, diastolic dysfunction
26 was attenuated as measured both by E/A wave ratio from pulse wave Doppler echocardiography (F-2HM-
27 AAV-scram: 1.99 ± 0.11 vs F-2HM-AAV9-*Runx1*: 1.49 ± 0.05, p = 0.0007 Figure 5i, Supplemental Figure

1 6), and by the slope of the EDPVR (F-2HM-AAV-scram: 0.082 ± 0.0002 vs F-2HM-AAV9-*Runx1*: $0.041 \pm$
2 0.0057 , $p = 0.0027$; Figure 5j, 5k).

3

4 **DISCUSSION**

5 This work identifies a critical role for RUNX1 in the development of HFpEF. Furthermore, we provide
6 evidence that targeting *Runx1* in the context of HFpEF has clinical translational potential.

7 In recent years, significant work has been done to establish a model with preserved EF which not
8 only demonstrates increased hypertrophy but also phenotypes such as pulmonary oedema, exercise
9 intolerance, and diastolic dysfunction and therefore is more representative of the multi-morbidity, multi-
10 system disorder of HFpEF in humans ^{20,24}.

11 *Runx1* has been robustly demonstrated to play an important role in the context of cardiac disease,
12 with a particular emphasis on its importance in adverse cardiac remodelling following MI ^{11,22,25,26}.
13 Previous work has demonstrated the beneficial effects of targeting *Runx1* in the context of acute MI ²² and
14 in the context of ischemic heart disease, however whether these benefits would be observed in a cardiac
15 syndrome of a chronic progressive nature such as HFpEF was unknown.

16 Therefore, we adapted a 2HM of HFpEF in our line of transgenic mice with cardiomyocyte *Runx1*
17 deficiency, and then again with the C57-N strain mice using translational approaches to target *Runx1*.
18 Overall, this work has identified RUNX1 as a promising new therapeutic target for treatment and
19 prevention of HFpEF.

20 Targeting *Runx1* with a cardiomyocyte-specific *Runx1*-deficient mouse attenuates the
21 development of a HFpEF phenotype. *Runx1*-deficiency is highly protective against the development of
22 HFpEF because despite the efficacy of the two-hits (*i.e.*, mice in both 2HM groups gained weight and had
23 increased SBP), the *Runx1*-deficient mice did not develop all the signs of HFpEF whereas control mice
24 had a classical HFpEF phenotype. Specifically, *Runx1*-deficiency reduced the development of
25 hypertrophy and exercise intolerance and completely protected against development of pulmonary
26 oedema and diastolic dysfunction. Although in this study we have simply targeted a single gene (*Runx1*)

1 in a single cell type (cardiomyocytes), the phenotypic outcome was evident systemically including effects
2 on exercise intolerance, pulmonary oedema, and the mass of peripheral organs, reflecting the beneficial
3 effects of targeting *Runx1* for both cardiac dysfunction and peripheral systems.

4 We corroborated these findings using RNAi. Interestingly, similar to the convincing protection of *Runx1*-
5 deficient mice, targeting *Runx1* with RNAi also protected mice against the development of diastolic
6 dysfunction and pulmonary oedema. While these results are promising, we utilized a preventive strategy,
7 which is not necessarily applicable to all clinical scenarios. An interventional approach was therefore used
8 by administering a small molecule RUNX1 inhibitor Ro5-3335, *after* the establishment of HFpEF. This
9 approach to inhibit *Runx1* demonstrated similar outcomes, albeit with fewer parameters affected. This
10 difference in outcomes may reflect the number of cardiomyocytes exposed to the intervention and/or,
11 effects on non-cardiomyocytes or duration of exposure. For example, the difference in cardiomyocyte
12 cross-sectional area despite the lack of change in LV mass in 2HM-AAV9-*Runx1* compared to 2HM-
13 AAV9-scram may be due to technical variability in LV isolation or may point to mechanistic differences,
14 such as increased extracellular matrix or interstitial content, or altered cellular composition. Future work
15 will aim to further understand the relative benefits of different approaches.

16 To interrogate potential gene changes underlying the phenotypic differences observed when
17 inhibiting *Runx1*, we used RNAseq. This resulted in predictions using IPA software for changes in the
18 regulation of diseases and functions when comparing the final time point (after 13 weeks of 2HM) tissue
19 in both groups compared to day 0 (D0) heart tissue. In any chronic disease it is difficult to determine at
20 which timepoint transcriptional changes might best be identified in order to discern differences between
21 *Runx1^{fl/fl}* and *Runx1^{Δ/Δ}* mice because relevant changes in the transcriptome may precede phenotype
22 differences. As such, it is perhaps unsurprising that the most DEG were shared between strains despite
23 the stark phenotypic differences between the 2HM transgenic groups. However, IPA did predict an
24 upregulation in congestive heart failure pathways in both *Runx1^{fl/fl}* and *Runx1^{Δ/Δ}* mice, with larger changes
25 occurring in *Runx1^{fl/fl}* compared to *Runx1^{Δ/Δ}* mice despite more gene changes overall occurring in the
26 *Runx1^{Δ/Δ}* mice. Interestingly, it was predicted that the upregulation of cardiac damage pathways would
27 result in larger changes in *Runx1^{Δ/Δ}* mice compared to *Runx1^{fl/fl}* mice.

1 Finally, we expanded the translational relevance of our work by performing a study to reverse
2 adverse cardiac remodelling in HFpEF in female mice. This enabled us to not only determine the effect of
3 gene transfer in both sexes but also interrogate the translational potential of targeting *Runx1* with AAV9
4 after the HFpEF phenotype was fully established (in contrast to our male study where AAV was
5 administered prior to mice being placed on the 2HM protocol). Overall, inhibiting *Runx1* via RNAi was
6 effective in reducing hypertrophy, pulmonary oedema, and reversing diastolic dysfunction in the female
7 2HM, thus indicating a potential role for *Runx1* in the treatment of HFpEF in both females as well as
8 males.

9 The aetiology of HFpEF and the associated changes in heart structure and diastolic function are
10 complex and relatively poorly understood. The relative contributions of the metabolic changes at a cellular
11 level and the chronic low-grade inflammation that accompanies metabolic stress and hypertension are not
12 clear. It is remarkable that the relatively simple model developed by Schiattarella *et al* in 2019 and used
13 again here can recapitulate many of the phenotypic changes associated with HFpEF given the subtleties
14 of these physiological insults and their complex interplay. We acknowledge that RUNX1 is likely to
15 modulate several aspects in the heart that mediate the pathogenesis of this syndrome. Notably, the
16 cardioprotection mediated by *Runx1* deficiency was independent of changes in blood pressure or body
17 weight, demonstrating that its beneficial effects are not mediated through the attenuation of primary
18 syndrome inducers but rather through direct modulation of the cardiac response to such stress. It is
19 intriguing that attenuation of *Runx1* function alleviates the deleterious effects observed both following MI
20 and prevents and reverses key aspects of HFpEF, hinting at a more fundamental role in the response of
21 heart damage and pathophysiological insult. It is plausible that RUNX1 acts as a maladaptive master
22 regulator across heart failure, with context-specific actions. In HFrEF, often driven by acute cardiac injury,
23 RUNX1 compromises systolic function⁶⁻⁸. In HFpEF, which is characterized by chronic metabolic and
24 hypertensive stress, it promotes diastolic dysfunction. This phenotypic divergence, may arise from
25 pathology-specific upstream signals engaging distinct transcriptional programs, as supported by our
26 RNAseq data. We however note that there are common pathways that are involved in both HFrEF and
27 HFpEF (abnormal calcium handling, mitochondrial function and inflammation/immune response) that
28 *Runx1* can target in both syndromes and is the focus of our future work.

1 Overall, this study clearly demonstrates that RUNX1 drives pathological changes in
2 cardiomyocytes in the context of HFpEF. Inhibition of *Runx1* by gene transfer or the use of a small
3 molecule inhibitor improves LV diastolic function and represents an exciting translational approach for the
4 treatment of HFpEF.

5 **LIMITATIONS**

6 To assess the role of *Runx1* in HFpEF, we induced HFpEF by increasing body weight and blood
7 pressure *via* administration of high fat diet and L-NAME. This limits our capacity to interrogate the role of
8 *Runx1* in the development of hypertension and obesity. In order to gain a more complete understanding of
9 the possible therapeutic potential of *Runx1*, further work will need to be performed to understand its
10 contribution to this complex and systemic syndrome, including the comorbidities associated with it, such
11 as diabetes and hypertension.

12 It is possible that many of the DEG in our bulk tissue samples will be the result of transcriptional
13 changes in non-cardiomyocyte cell types in the ventricle, potentially diluting cardiomyocyte-specific
14 changes that are the result of the *Runx1*-deficiency. Single-cell transcriptomic analysis, potentially at
15 multiple time points, is part of the programme of future work.

16 Additionally, AAV9-mediated *Runx1* knockdown approach in male mice was prophylactic, which
17 does not mirror a typical clinical scenario albeit the female study clearly demonstrates that inhibition of
18 *Runx1* can reverse diastolic dysfunction in HFpEF. Furthermore, the small-molecule inhibitor Ro5-3335,
19 while administered after onset of the HFpEF phenotype, showed a more restricted improvement, primarily
20 reversing diastolic dysfunction and reducing pulmonary oedema. We note also that echocardiographic
21 assessment of diastolic function was performed without simultaneous ECG recording and exercise
22 capacity was not normalized to body weight and should be taken into consideration in future studies
23 exploring the benefits of *Runx1* inhibitors in cardiac disease.

24 **ACKNOWLEDGMENTS**

25 The authors thank Michael Dunne, Margaret Bell, and Catherine Hawksby and the Biological Services
26 staff from the University of Glasgow Cardiovascular Research Unit for their surgical, animal, and technical

1 assistance. We thank Douglas Strathdee, the Transgenic Technologies Lab, BSU and Histology lab at the
2 Beatson Institute.

3 **FUNDING**

4 This work was supported by a BHF programme grant RG/20/6/35095 to C.L., E.C, S.N. and C. B. C.B.
5 and C.M.L were also supported by the British Heart Foundation (RE/18/6/34217).

6 **DISCLOSURE OF INTEREST**

7 Authors have nothing to disclose.

8 **DATA AVAILABILITY STATEMENT**

9 Data from this study are available upon request to the corresponding author.

10 **REFERENCES**

- 11 1. Desai N, Olewinska E, Famulska A, Remuzat C, Francois C, Folkerts K. Heart failure with mildly
12 reduced and preserved ejection fraction: A review of disease burden and remaining unmet medical
13 needs within a new treatment landscape. *Heart Fail Rev.* 2024;29:631–662.
- 14 2. Tsao CW, Lyass A, Enserro D, Larson MG, Ho JE, Kizer JR, Gottdiener JS, Psaty BM, Vasan RS.
15 Temporal trends in the incidence of and mortality associated with heart failure with preserved and
16 reduced ejection fraction. *JACC Heart Fail.* 2018;6:678–685.
- 17 3. Dunlay SM, Roger VL, Redfield MM. Epidemiology of heart failure with preserved ejection fraction.
18 *Nat Rev Cardiol.* 2017;14:591–602.
- 19 4. Omote K, Verbrugge FH, Borlaug BA. Heart failure with preserved ejection fraction: mechanisms
20 and treatment strategies. *Annu Rev Med.* 2022;73:321–337.
- 21 5. Mishra S, Kass DA. Cellular and molecular pathobiology of heart failure with preserved ejection
22 fraction. *Nat Rev Cardiol.* 2021;18:400–423.
- 23 6. McCarroll CS, He W, Foote K, Bradley A, McGlynn K, Vidler F, Nixon C, Nather K, Fattah C,
24 Riddell A, et al. Runx1 deficiency protects against adverse cardiac remodeling after myocardial
25 infarction. *Circulation.* 2018;137:57–70.
- 26 7. Riddell A, McBride M, Braun T, Nicklin SA, Cameron E, Loughrey CM, Martin TP. RUNX1: An
27 emerging therapeutic target for cardiovascular disease. *Cardiovasc Res.* 2020;116:1410–1423.
- 28 8. Li X, Zhang S, Wa M, Liu Z, Hu S. MicroRNA-101 Protects Against Cardiac Remodeling Following
29 Myocardial Infarction via Downregulation of Runt-Related Transcription Factor 1. *J Am Heart*
30 *Assoc.* 2019;8:1–16.

- 1 9. Zhang D, Liang C, Li P, Yang L, Hao Z, Kong L, Tian X, Guo C, Dong J, Zhang Y, et al. Runx1-related transcription factor 1 (Runx1) aggravates pathological cardiac hypertrophy by promoting
2 p53 expression. *J Cell Mol Med.* 2021;25:7867–7877.
3
- 4 10. Qi P, Zhai Q, Zhang X. RUNX1 facilitates heart failure progression through regulating TGF- β -
5 induced cardiac remodeling. *PeerJ.* 2023;11.
- 6 11. Li P, Jia XY. MicroRNA-18-5p inhibits the oxidative stress and apoptosis of myocardium induced by
7 hypoxia by targeting RUNX1. *Eur Rev Med Pharmacol Sci.* 2022;26:432–439.
- 8 12. Tzimas C, Rau CD, Buergisser PE, Jean-Louis G, Lee K, Chukwunkeke J, Dun W, Wang Y, Tsai EJ.
9 WIP1 is a conserved mediator of right ventricular failure. *JCI Insight.* 2019;5.
- 10 13. Yamaguchi T, Sumida TS, Nomura S, Satoh M, Higo T, Ito M, Ko T, Fujita K, Sweet ME, Sanbe A,
11 et al. Cardiac dopamine D1 receptor triggers ventricular arrhythmia in chronic heart failure. *Nat*
12 *Commun.* 2020;11:4364.
- 13 14. Yang G, Chen S, Ma A, Lu J, Wang T. Identification of the difference in the pathogenesis in heart
14 failure arising from different etiologies using a microarray dataset. *Clinics (Sao Paulo).*
15 2017;72:600–608.
- 16 15. Tan WLW, Anene-Nzulu CG, Wong E, Lee CJM, Tan HS, Tang SJ, Perrin A, Wu KX, Zheng W,
17 Ashburn RJ, et al. Epigenomes of Human Hearts Reveal New Genetic Variants Relevant for
18 Cardiac Disease and Phenotype. *Circ Res.* 2020;127:761–777.
- 19 16. Sun N, Yazawa M, Liu J, Han L, Sanchez-Freire V, Abilez OJ, Navarrete EG, Hu S, Wang L, Lee
20 A, et al. Patient-specific induced pluripotent stem cells as a model for familial dilated
21 cardiomyopathy. *Sci Transl Med.* 2012;4:130ra47.
- 22 17. Perestrelo AR, Silva AC, Oliver-De La Cruz J, Martino F, Horvath V, Caluori G, Polansky O,
23 Vinarsky V, Azzato G, De Marco G, et al. Multiscale Analysis of Extracellular Matrix Remodeling in
24 the Failing Heart. *Circ Res.* 2021;128:24–38.
- 25 18. Edgar R, Domrachev M, Lash AE. Gene Expression Omnibus: NCBI gene expression and
26 hybridization array data repository. *Nucleic Acids Res.* 2002;30:207–10.
- 27 19. Zile MR, Baicu CF, Ikonomidis JS, Stroud RE, Nietert PJ, Bradshaw AD, Slater R, Palmer BM, Van
28 Buren P, Meyer M, et al. Myocardial stiffness in patients with heart failure and a preserved ejection
29 fraction: contributions of collagen and titin. *Circulation.* 2015;131:1247–59.
- 30 20. Schiattarella GG, Altamirano F, Tong D, French KM, Villalobos E, Kim SY, Luo X, Jiang N, May HI,
31 Wang Z V., et al. Nitrosative stress drives heart failure with preserved ejection fraction. *Nature.*
32 2019;568:351–356.
- 33 21. Gowney JD, Shigematsu H, Li Z, Lee BH, Adelsperger J, Rowan R, Curley DP, Kutok JL, Akashi
34 K, Williams IR, et al. Loss of Runx1 perturbs adult hematopoiesis and is associated with a
35 myeloproliferative phenotype. *Blood.* 2005;106:494–504.
- 36 22. Martin TP, MacDonald EA, Bradley A, Watson H, Saxena P, Rog-Zielinska EA, Raheem A, Fisher
37 S, Elbassioni AAM, Almuzaini O, et al. Ribonucleic acid interference or small molecule inhibition of
38 Runx1 in the border zone prevents cardiac contractile dysfunction following myocardial infarction.
39 *Cardiovasc Res* [Internet]. 2023;1–9. Available from:
40 <https://academic.oup.com/cardiovasces/advance-article/doi/10.1093/cvr/cvad107/7222852>

- 1 23. Tong D, Schiattarella GG, Jiang N, May HI, Lavandro S, Gillette TG, Hill JA. Female Sex Is
2 Protective in a Preclinical Model of Heart Failure with Preserved Ejection Fraction. *Circulation*.
3 2019;140:1769–1771.
- 4 24. Masiukevich D, Kovacs A, Li T, Kokkonen-Simon K, Matkovich SJ, Oladipupo SS, Ornitz DM.
5 Characterization of a robust mouse model of heart failure with preserved ejection fraction. *Am J*
6 *Physiol Heart Circ Physiol* [Internet]. 2023;325:H203–H231. Available from:
7 <http://www.ncbi.nlm.nih.gov/pubmed/37204871>
- 8 25. Liu X, Yin K, Chen L, Chen W, Li W, Zhang T, Sun Y, Yuan M, Wang H, Song Y, et al. Lineage-
9 specific regulatory changes in hypertrophic cardiomyopathy unraveled by single-nucleus RNA-seq
10 and spatial transcriptomics. *Cell Discov* [Internet]. 2023;9:6. Available from:
11 <http://www.ncbi.nlm.nih.gov/pubmed/36646705>
- 12 26. Ni T, Huang X, Pan S, Lu Z. Dihydrolycorine Attenuates Cardiac Fibrosis and Dysfunction by
13 Downregulating Runx1 following Myocardial Infarction. *Oxid Med Cell Longev*. 2021;2021.

Figure 1. *Runx1*-deficient mice are protected against HFpEF phenotype. **A)** Schematic of two-hit protocol and experimental groups. **B)** Body weight over the experimental protocol in each of the groups. * $p < 0.05$ for 2HM-*Runx1*^{fl/fl} (n = 21) compared to CTRL-*Runx1*^{fl/fl} (n = 19), # $p < 0.05$ for 2HM-*Runx1*^{Δ/Δ} (n = 22) compared to CTRL-*Runx1*^{Δ/Δ} (n = 17), and † $p < 0.05$ for 2HM-*Runx1*^{Δ/Δ} compared to 2HM-*Runx1*^{fl/fl} by mixed-effects analysis. **C)** Systolic blood pressure (BP) over the experimental protocol. * $p < 0.05$ for 2HM-*Runx1*^{fl/fl} (n = 25) compared to CTRL-*Runx1*^{fl/fl} (n = 18) and # $p < 0.05$ for 2HM-*Runx1*^{Δ/Δ} (n = 19) compared to CTRL-*Runx1*^{Δ/Δ} (n = 25) by mixed-effects analysis. Characterisation of the HFpEF phenotype: **D)** Exercise intolerance was quantified by running distance (CTRL-*Runx1*^{fl/fl}: n = 5; CTRL-*Runx1*^{Δ/Δ}: n = 7; 2HM-*Runx1*^{fl/fl}: n = 12; 2HM-*Runx1*^{Δ/Δ}: n = 8) by mixed-effects analysis. **E)** Pulmonary oedema quantified by wet to dry lung weight ratio (CTRL-*Runx1*^{fl/fl}: n = 10; CTRL-*Runx1*^{Δ/Δ}: n = 11; 2HM-*Runx1*^{fl/fl}: n = 11; 2HM-*Runx1*^{Δ/Δ}: n = 11) by two-way ANOVA. Hypertrophy was quantified by **f)** left ventricular (LV) weight (CTRL-*Runx1*^{fl/fl}: n = 12; CTRL-*Runx1*^{Δ/Δ}: n = 13; 2HM-*Runx1*^{fl/fl}: n = 12; 2HM-*Runx1*^{Δ/Δ}: n = 13) by two-way ANOVA and by **g)** cardiomyocyte cross sectional area assessed following Wheat Germ Agglutinin staining (CTRL-*Runx1*^{fl/fl}: n = 4; CTRL-*Runx1*^{Δ/Δ}: n = 4; 2HM-*Runx1*^{fl/fl}: n = 5; 2HM-*Runx1*^{Δ/Δ}: n = 5) by two-way ANOVA. Diastolic function quantified by **h)** E to A wave ratio from pulsed wave Doppler echocardiography (CTRL-*Runx1*^{fl/fl}: n = 5; CTRL-*Runx1*^{Δ/Δ}: n = 6; 2HM-*Runx1*^{fl/fl}: n = 4; 2HM-*Runx1*^{Δ/Δ}: n = 5) by two-way ANOVA and by the slope (β) of the end-diastolic pressure volume relationship derived from the exponential equation: LVEDP = curve fitting constant $\times e^{[\text{stiffness constant} \times \text{LV end diastolic volume}]}$. **i)** representative curves (error lines denote 95% confidence interval; and **j)** data set (2HM-*Runx1*^{fl/fl}: n = 9; 2HM-*Runx1*^{Δ/Δ}: n = 8) by t-test.

Figure 2. AAV9-mediated knockdown of *Runx1* protects against diastolic dysfunction. **A)** Schematic of two-hit protocol and experimental groups. **B)** Body weight over the experimental protocol i* $p < 0.05$ for 2HM C57N (n = 18) compared to CTRL-C57N (n = 13), # $p < 0.05$ for 2HM-AAV9-scrum (n = 10) compared to CTRL-C57N, and † $p < 0.05$ for 2HM-AAV9-*Runx1* (n = 11) compared to CTRL-C57N by mixed-effects analysis. **C)** Systolic blood pressure (BP) over the experimental protocol. * $p < 0.05$ for 2HM-C57N (n = 38) compared to CTRL-C57N (n = 31), # $p < 0.05$ for 2HM-AAV9-scrum (n = 10) compared to CTRL-C57N, and † $p < 0.05$ for 2HM-AAV9-*Runx1* (n = 10) compared to CTRL-C57N by mixed-effects analysis. Characterisation of the HFpEF phenotype: **D)** Exercise intolerance was quantified by running distance (CTRL-C57N: n = 6; 2HM-C57N: n = 4; 2HM-AAV9-scrum: n = 8; 2HM-AAV9-*Runx1*: n = 10) by one-way ANOVA. **E)** Pulmonary oedema quantified by wet to dry lung weight ratio (CTRL-C57N: n = 13; 2HM-C57N: n = 13; 2HM-AAV9-scrum: n = 10; 2HM-AAV9-*Runx1*: n = 11) by one-way ANOVA. Hypertrophy was quantified by **F)** left ventricular (LV) weight normalised to tibial length (TL) (CTRL-C57N: n = 14; 2HM-C57N: n = 20; 2HM-AAV9-scrum: n = 10; 2HM-AAV9-*Runx1*: n = 11) by one-way ANOVA and by **G)** cardiomyocyte cross sectional area assessed following Wheat Germ Agglutinin staining (2HM-AAV9-scrum: n = 5; 2HM-AAV9-*Runx1*: n = 5) by t-test. Diastolic function quantified by E to A wave ratio from pulsed wave Doppler echocardiography (CTRL-C57N: n = 12; 2HM-C57N: n = 6; 2HM-AAV9-scrum: n = 9; 2HM-AAV9-*Runx1*: n = 13) on **H)** the final week by one-way ANOVA and **i)** over the protocol by two-way ANOVA; and by the slope (β) of the end-diastolic pressure volume relationship derived from the exponential equation: (LVEDP = curve fitting constant $\times e^{[\text{stiffness constant} \times \text{LV end diastolic volume}]}$), 2HM-AAV9-scrum: n = 5; 2HM-AAV9-*Runx1*: n = 6. **j)** representative curves (error lines denote 95% confidence interval; and **k)** data set by t-test.

1
2

Figure 3. *Runx1* small molecule inhibitor Ro5-3335 remedies against diastolic dysfunction. **A)** Schematic of two-hit protocol and experimental groups, 2HM-DMSO (n = 12) and 2HM-Ro5-3335 (n = 14). Characterisation of the HFpEF phenotype: **B)** Exercise intolerance was quantified by running distance, pre- and post-treatment (2HM-DMSO: n = 8; 2HM-Ro5-3335: n = 8) by t-test. **C)** Pulmonary oedema was quantified by wet to dry lung weight ratio (2HM-DMSO: n = 12; 2HM-Ro5-3335: n = 14) by t-test. Hypertrophy was quantified by **D)** left ventricular (LV) weight normalised to tibial length (TL) (2HM-DMSO: n = 12; 2HM-Ro5-3335: n = 14) by t-test. Diastolic function quantified by **E)** E to A wave ratio from pulsed wave Doppler echocardiography, pre- and post-treatment (2HM-DMSO: n = 9; 2HM-Ro5-3335: n = 10) by t-test and by the slope (β) of the end-diastolic pressure volume relationship derived from the exponential equation: (LVEDP= curve fitting constant $\times e^{[\text{stiffness constant} \times \text{LV end diastolic volume}]}$) 2HM-DMSO: n = 7; 2-HM-Ro5-3335; n = 6 by t-test. **F)** representative curves (error lines denote 95% confidence interval; and **g)** data set by t-test.

Figure 4. Cardiac differential gene expression (DEG) analysis of *Runx1*^{fl/fl} and *Runx1* ^{$\Delta\Delta$} mice between day 0 (D0) and 13 weeks of two-hit model (2HM) protocol. Volcano plots of all genes (orange-significantly downregulated, green-significantly upregulated and grey not changing) with the eight most regulated genes indicated in **a)** *Runx1*^{fl/fl} (CTRL: n = 6; 2HM: n = 6) and **b)** *Runx1* ^{$\Delta\Delta$} mice (CTRL: n = 6; 2HM: n = 6). **c)** Venn diagram indicating unique changes and the large number of genes that are commonly differentially regulated between group comparison. **d)** Differences in functional predictions using Z-scores comparing *Runx1*^{fl/fl} mice to *Runx1* ^{$\Delta\Delta$} mice (red indicating an activation between *Runx1*^{fl/fl} minus *Runx1* ^{$\Delta\Delta$} , blue indicating an inhibition, and yellow indicating similar functional predictions in both groups). Heat map representing patterns of **e)** congestive heart failure and **f)** cardiac damage gene expression levels between *Runx1*^{fl/fl} mice to *Runx1* ^{$\Delta\Delta$} mice.

Figure 5. AAV9-mediated knockdown of *Runx1* in female mice: partial reversal of HFpEF phenotype. **A)** Schematic of two-hit protocol and experimental groups, F-CTRL-C57N (n = 4), F-2HM-C57N (n = 16: F2HM-AAV-scram: n = 8; F2HM-AAV-*Runx1*: n = 8). **B)** Body weight (F-CTRL-C57N: n = 4; F-2HM-C57N, n = 17) by t-test. **C)** systolic blood pressure (BP) (F-CTRL-C57N: n = 4; F-2HM-C57N: n = 15) by t-test. **D)** exercise intolerance testing quantified by running distance (F-CTRL-C57N: n = 3; F-2HM-C57N: n = 16) by t-test. Diastolic function quantified by **E)** E to A wave ratio from pulsed wave Doppler echocardiography at week 8 (F-CTRL-C57N: n = 3; F-2HM-C57N: n = 16) by t-test. Post-injection, **F)** exercise intolerance was quantified by running distance (F-2HM-scram: n = 8; F-2HM-*Runx1*: n = 8) by t-test. **G)** Pulmonary oedema quantified by wet to dry lung weight ratio following removal of outlier identified by ROUT outlier test (F-2HM-scram: n = 8; F-2HM-*Runx1*: n = 7). Hypertrophy was quantified by **H)** left ventricular (LV) weight normalised to tibial length (TL) (F-2HM-scram: n = 8; F-2HM-*Runx1*: n = 8) by t-test. Diastolic function quantified by **i)** E to A wave ratio from pulsed wave Doppler echocardiography (F-2HM-scram: n = 8; F-2HM-*Runx1*: n = 8) and by the slope (β) of the end-diastolic pressure volume relationship derived from the exponential equation: LVEDP= curve fitting constant $\times e^{[\text{stiffness constant} \times \text{LV end diastolic volume}]}$ (F-2HM-scram: n = 3; F-2HM-*Runx1*: n = 5) by t-test. **F)** representative curves (error lines denote 95% confidence interval; and **g)** data set by t-test.

1
2
3

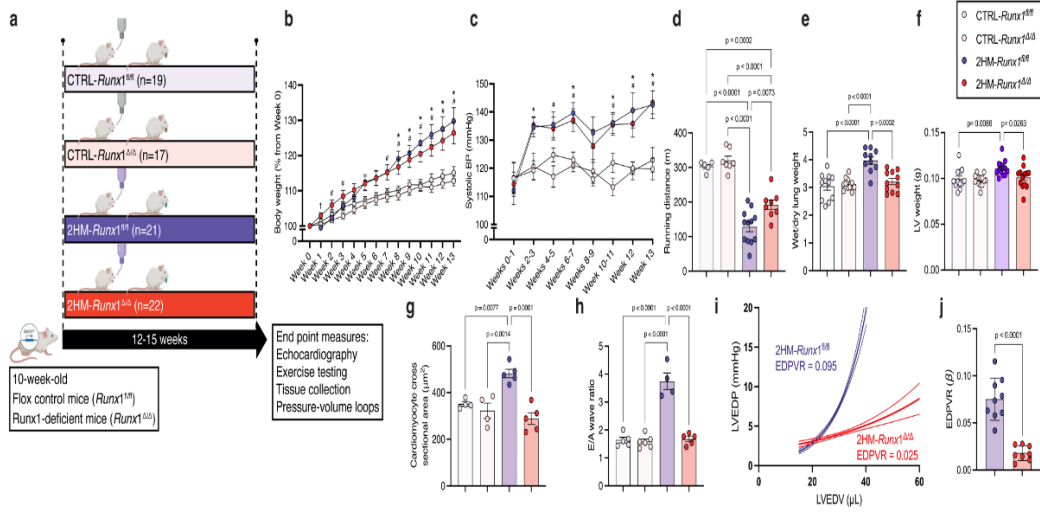


Figure 1
297x101 mm (x DPI)

1
2
3
4

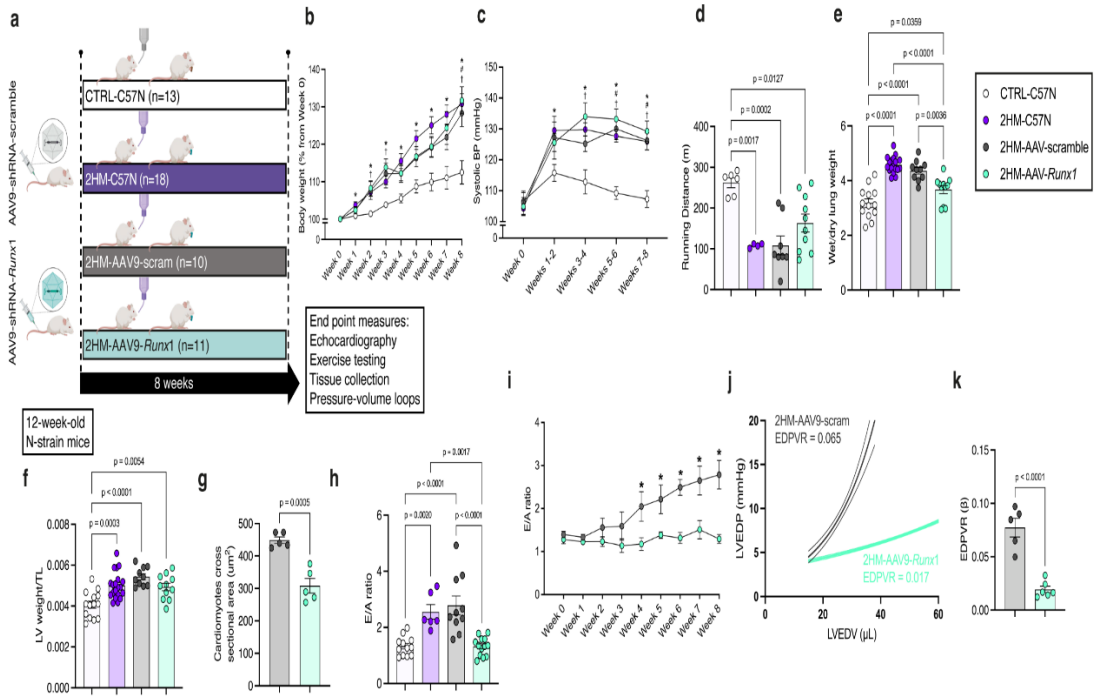
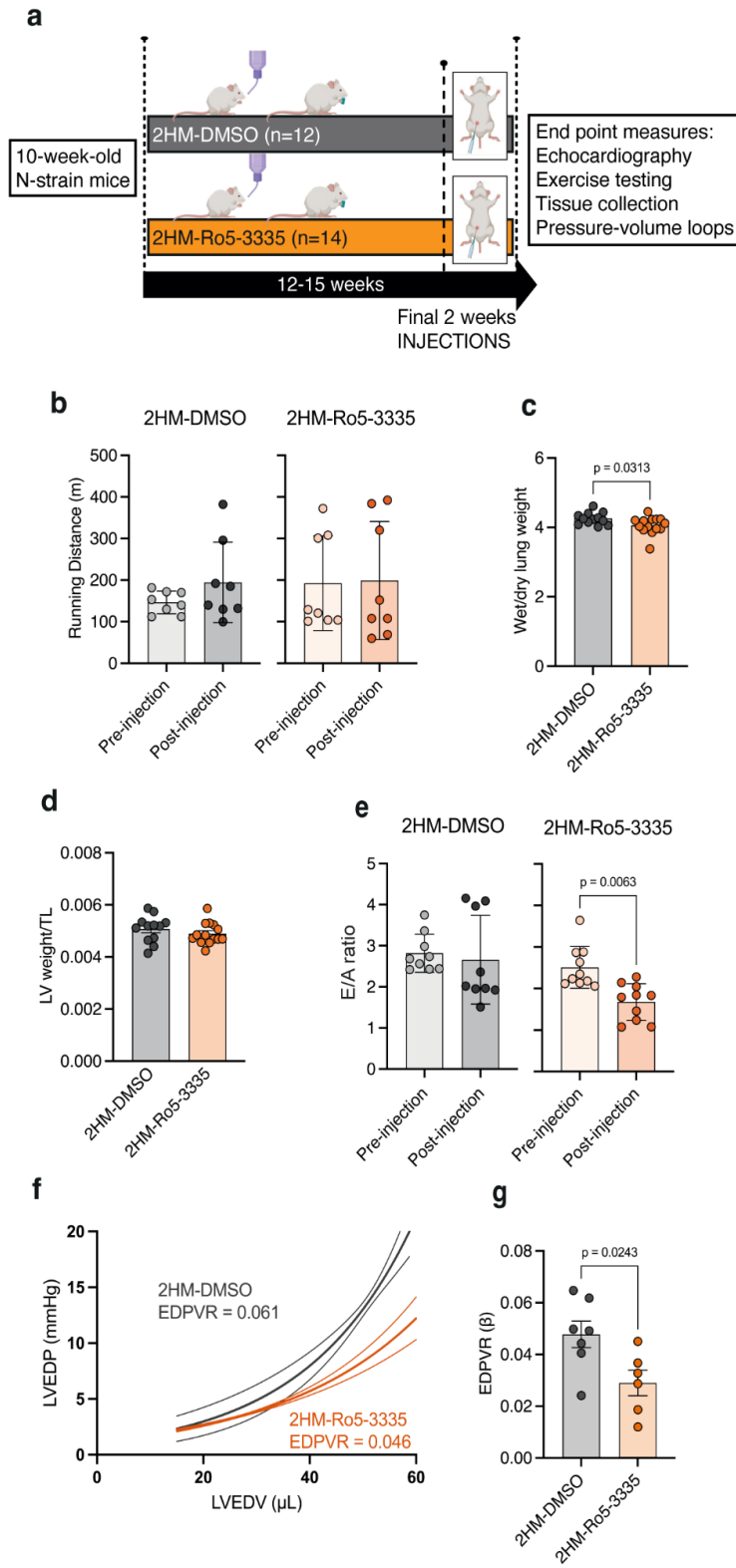


Figure 2
291x123 mm (x DPI)

5
6
7
8



1
2
3
4

Figure 3
112x223 mm (x DPI)

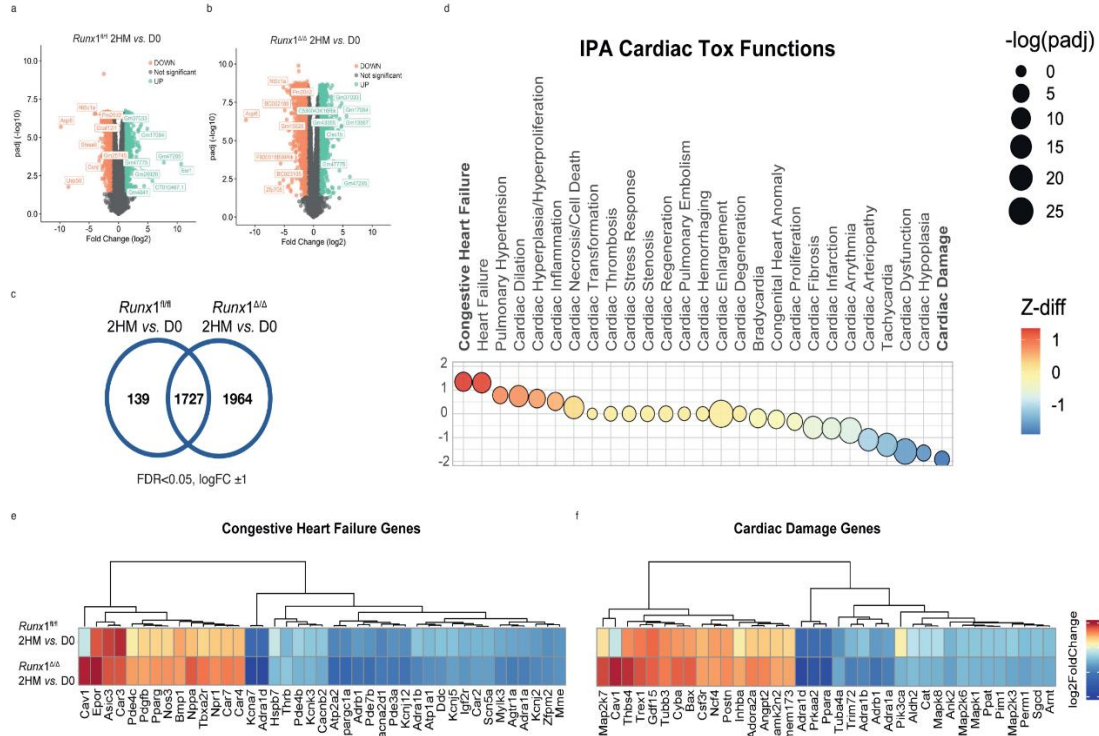


Figure 4
 275x167 mm (x DPI)

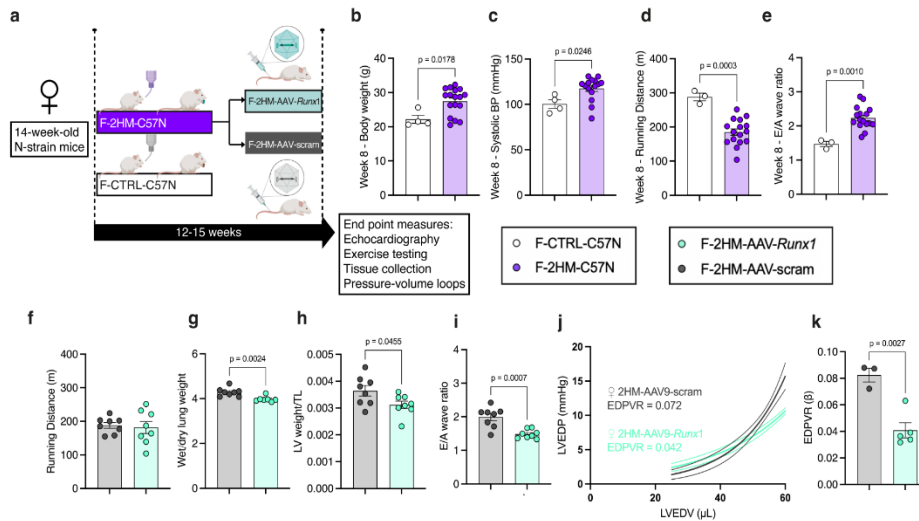
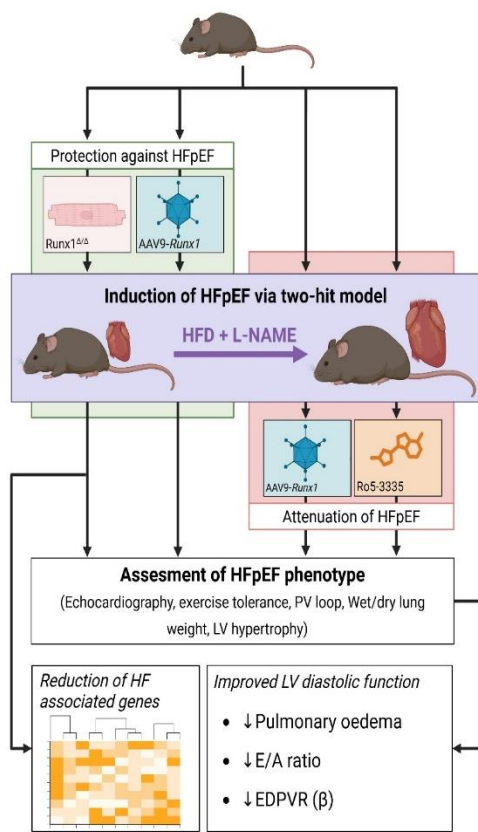


Figure 5
 225x119 mm (x DPI)



1
2
3

Graphical Abstract
254x178 mm (x DPI)